

Photochemical strategies for green synthesizing ultrathin Au nanosheets using photoinduced free radical generation and their catalytic properties

Suisui He, Jun Hai, Tianrong Li, Sha Liu, Fengjuan Chen,* Baodui Wang,*

State Key Laboratory of Applied Organic Chemistry Lanzhou University and Key Laboratory of Nonferrous Metal Chemistry and Resources Utilization of Gansu Province Lanzhou University, Lanzhou 730000, P.R. China. E-mail: litr@lzu.edu.cn; wangbd@lzu.edu.cn.

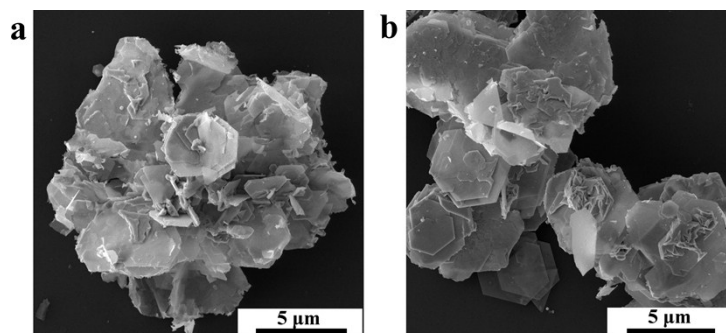


Figure S1. (a, b) SEM images of Au nanosheets obtained at different HAuCl₄ concentrations: (a) 0.8 mM HAuCl₄; (b) 1.0 mM HAuCl₄.

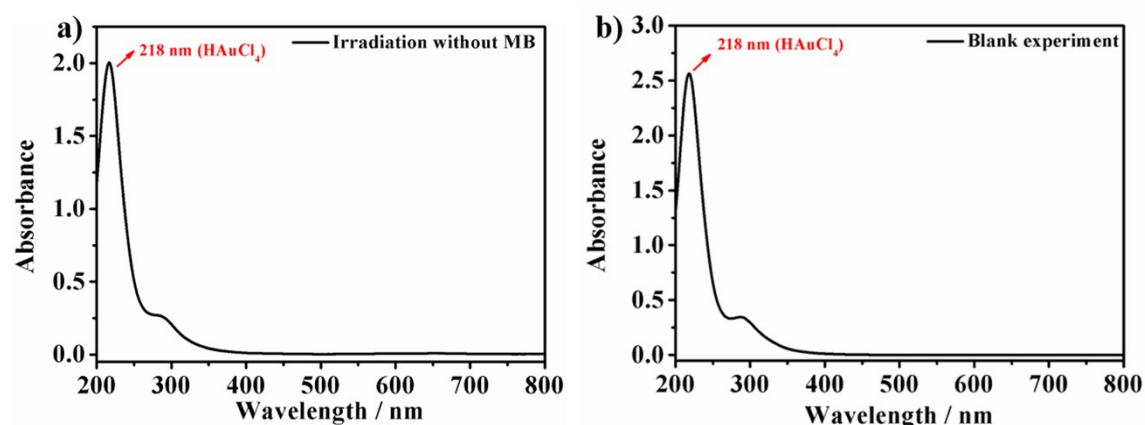


Figure S2. UV-vis spectrum of HAuCl₄ after visible light irradiation for 1 h (a) and HAuCl₄ without illumination (b). In the UV-vis spectrum, HAuCl₄ after visible light irradiation for 1 h and HAuCl₄ without illumination showed the same absorption peak of HAuCl₄ at 218 nm indicates that no Au nanosheets or nanoparticles were formed in the absence of MB.

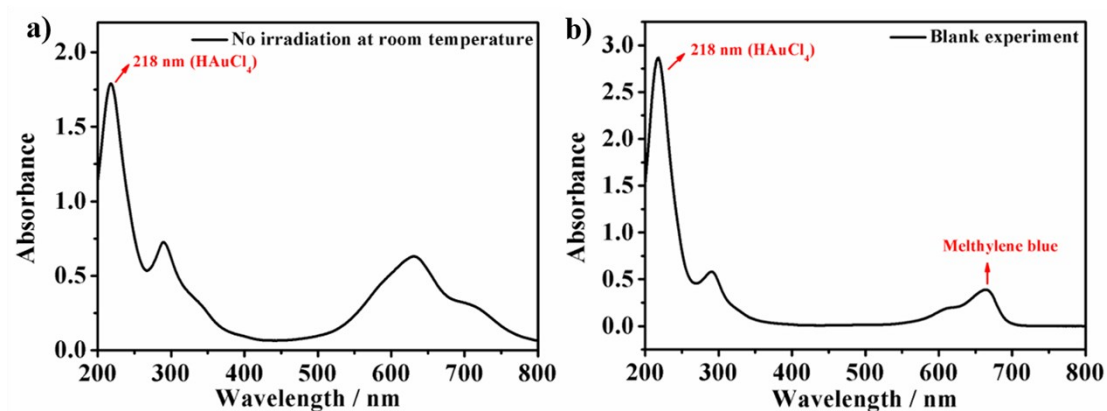


Figure S3. UV-vis spectrum of HAuCl₄ and Methylene blue (MB) without illumination at room temperature (a) and freshly prepared HAuCl₄ and MB (b). In the UV-vis spectrum, HAuCl₄ and MB without illumination at room temperature and freshly prepared HAuCl₄ and MB showed the same absorption peak of HAuCl₄ at 218 nm indicates that no Au nanosheets or nanoparticles were formed without illumination at room temperature.

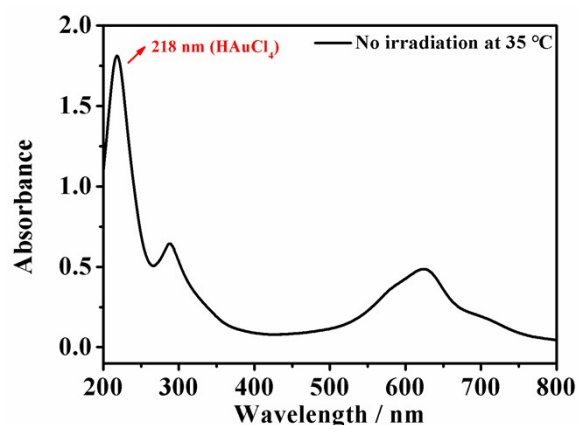
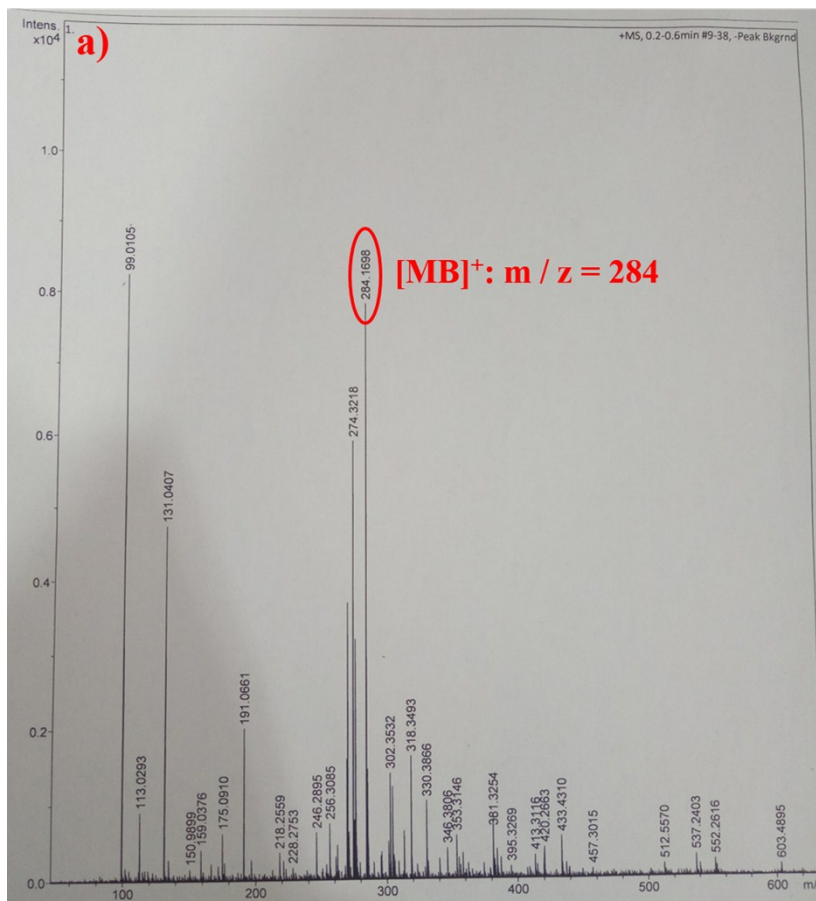
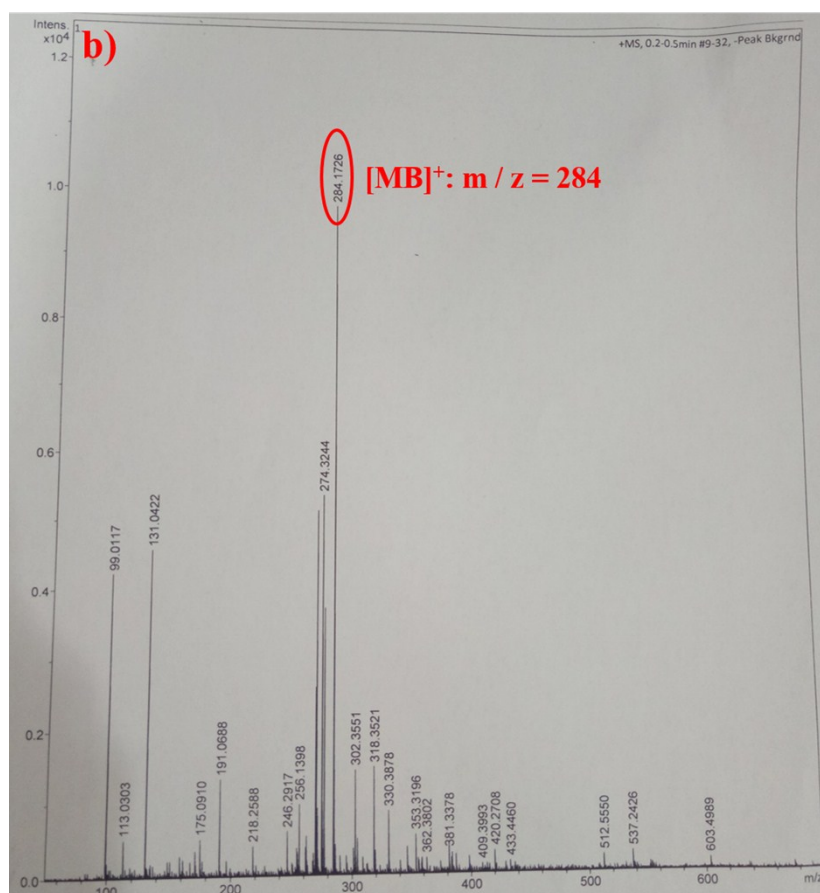


Figure S4. UV-vis spectrum of HAuCl₄ and MB at 35 °C in the dark for 1h. In the UV-vis spectrum, the reaction solution incubated at 35 °C in the dark for 1 h showed the absorption peak of HAuCl₄ at 218 nm indicates that no Au nanosheets or nanoparticles were formed at 35 °C.





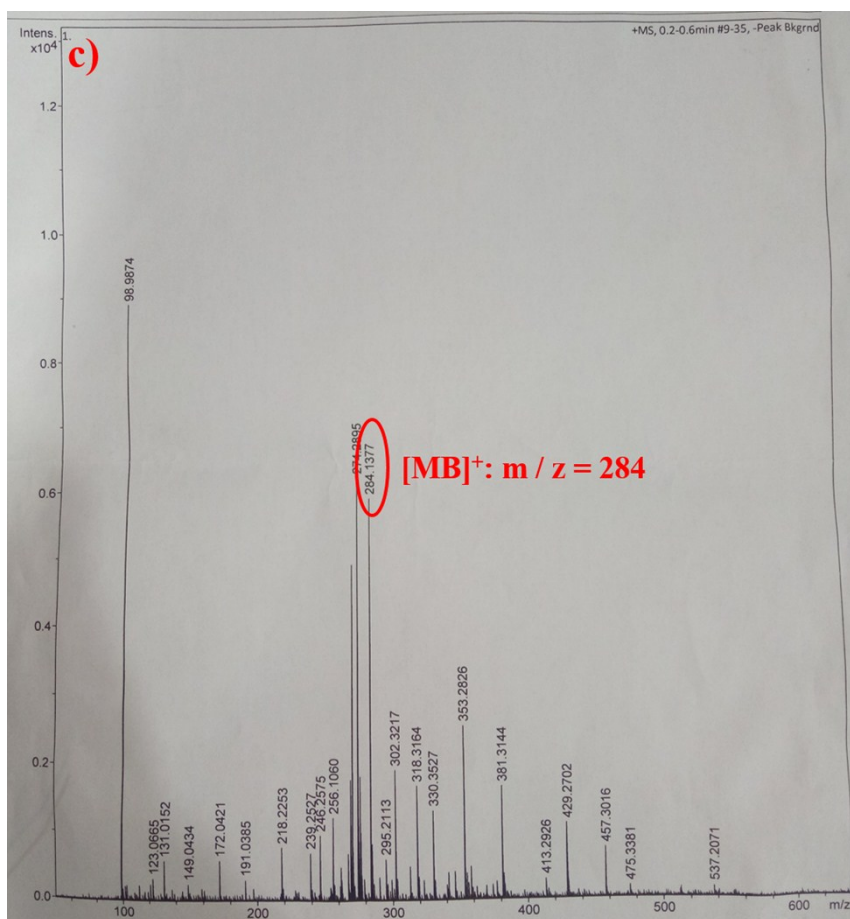


Figure S5. Mass spectrometry of MB in the solution during the formation of Au nanosheets obtained under different irradiation time: (a) 15 min; (b) 30 min; (c) 1 h. As shown in Figure S5, MB is always present in the reaction solution during the irradiation process.

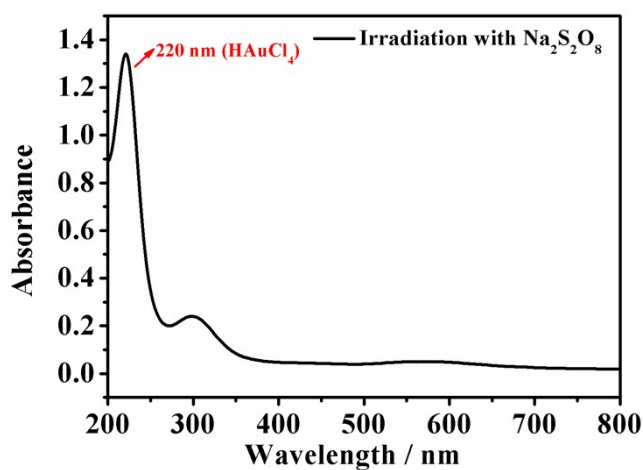


Figure S6. UV-vis spectrum of HAuCl_4 , $\text{Na}_2\text{S}_2\text{O}_8$ and MB under visible light irradiation for 1 h. In the UV-vis spectrum, HAuCl_4 , $\text{Na}_2\text{S}_2\text{O}_8$ and MB with illumination showed the absorption peak of HAuCl_4 at 220 nm indicates no Au nanosheets or nanoparticles were observed and also indicated that MB radicals were employed to generate nanosheets.

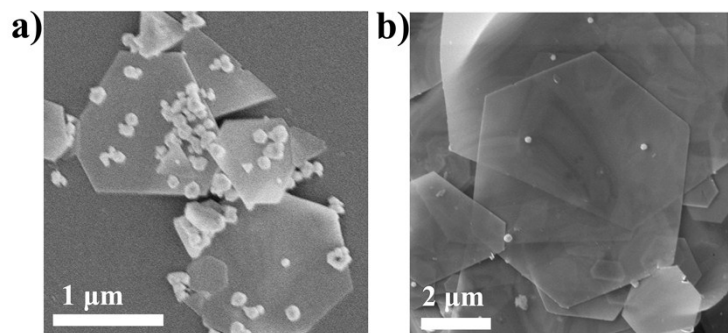


Figure S7. SEM images of Au nanosheets obtained using (a) 0.8 nmol MB (b) 3.2 nmol MB.

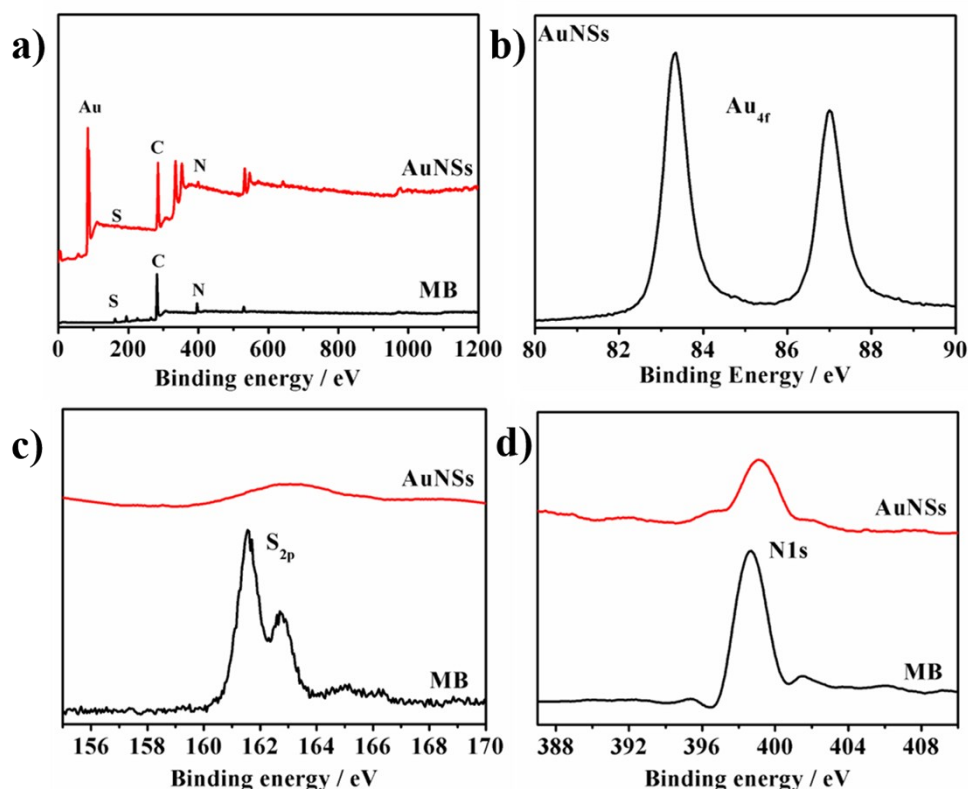


Figure S8. X-ray photoelectron spectroscopy (XPS) analysis¹ of Au nanosheets and MB. (a) Survey scan of the surface of Au nanosheets and MB, expanded spectra of (b) Au_{4f}, (c) S_{2p}, and (d) N_{1s}. The Au nanosheets were analyzed by XPS for the purpose of ascertaining the chemical composition of its surface. As shown in Figure S8a, the resulting Au nanosheets existed Au, C, N, and S element, and the C, N, and S element arised from MB. As shown in Figure S8c, the upshift of the S_{2p} from 161.54 eV for MB to 163.09 eV for Au nanosheets was attributed to the coordination of sulfur atoms to gold. Similarly, the upshift of the N_{2p} increases from 398.625 eV for MB to 399.12 eV for Au nanosheets also suggested N element coordination onto Au Nanosheets. In the case of Au nanosheets (Figure S8b), the peaks observed at binding energies of 83.31 and 87.01eV correspond to Au⁰ species. The results demonstrate that MB is anchored on the surfaces of the Au nanosheets after reaction.

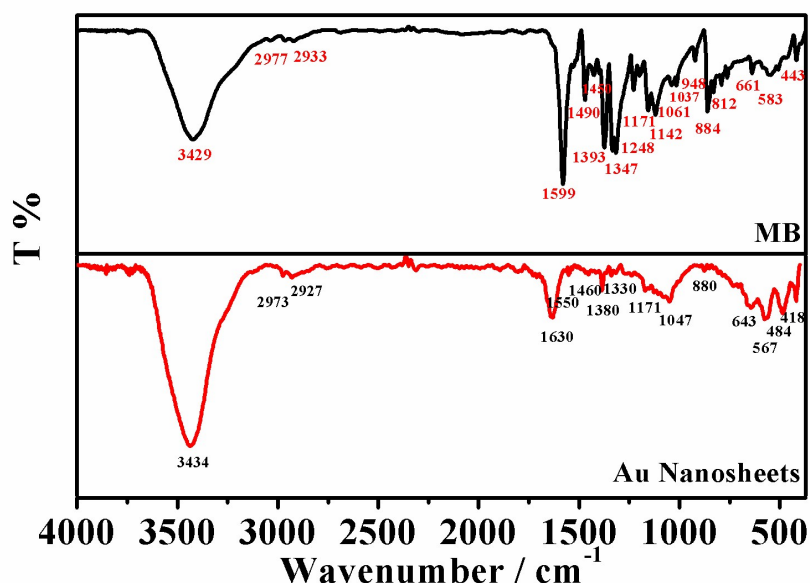


Figure S9. Fourier transform infrared spectroscopy (FTIR) spectra of MB (black) and Au nanosheets (red). In the IR spectrum of MB, peak at 3429 cm^{-1} corresponded to the absorption band of H_2O . And the absorption bands of the $\text{C}=\text{N}$ vibrations and benzene ring appeared at 1450 cm^{-1} , 1490 cm^{-1} and 1599 cm^{-1} . Moreover, peaks at 1142 cm^{-1} and 1037 cm^{-1} attributed to $\text{C}-\text{S}$ absorption bands. After the formation of Au nanosheets, the characteristic bands of $\text{C}=\text{N}$ and $\text{C}-\text{S}$ disappeared. Furthermore, the other characteristic bands of MB were also changed a little. In the IR spectrum of Au nanosheets, the Au-N absorption bands appeared at 484 cm^{-1} .² Our spectroscopic window extends to 400 cm^{-1} , and thus we cannot observe at this time such low-frequency vibrations as the Au-S stretch.³ Combining the XPS and FTIR spectra analysis, we can conclude that the N and S atoms coordinated with Au atom.

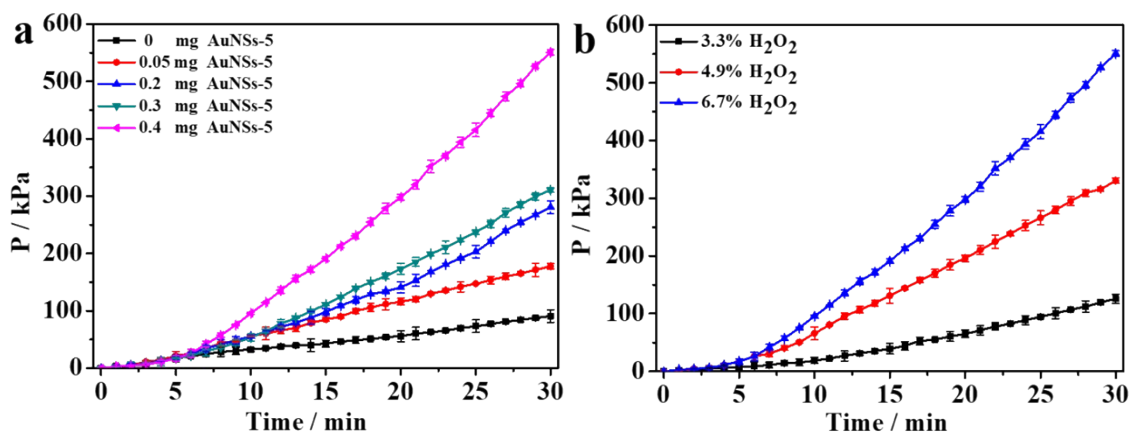


Figure S10. (a) Pressure-change profiles of the H_2O_2 decomposition reaction with different amounts of Au nanosheets catalase in 6.7% H_2O_2 solution. Pressure-change profiles of the H_2O_2 decomposition reaction at different H_2O_2 concentrations ($[\text{catalase}]=0.4\text{ mg}$).

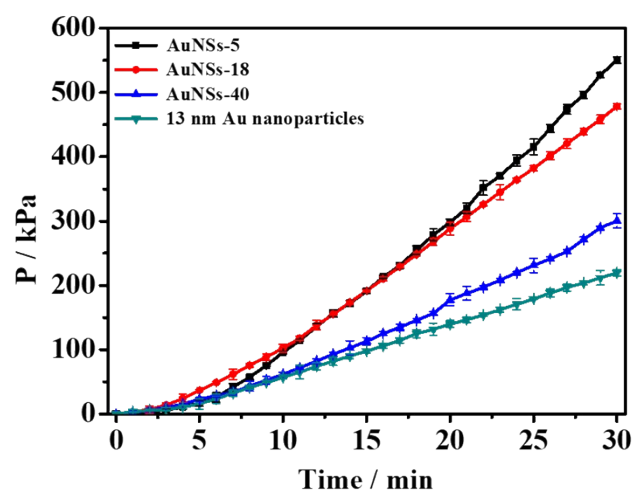


Figure S11. Pressure-change profiles of the H_2O_2 decomposition reaction with different thickness of Au nanosheets catalase and 13 nm Au nanoparticles in 6.7% H_2O_2 solution ([catalase]=0.4 mg). Values are expressed as mean \pm SD.

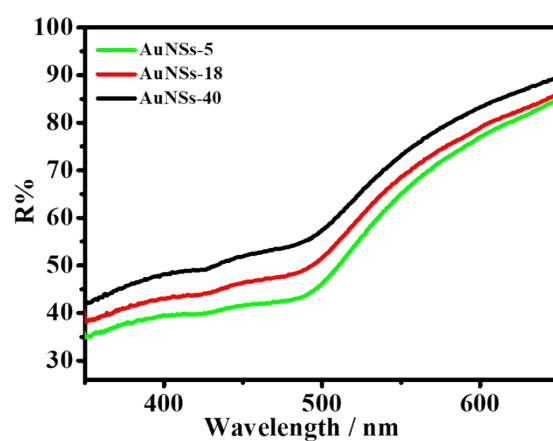


Figure S12. Reflection spectra of AuNSs-5, AuNSs-18 and AuNSs-40.

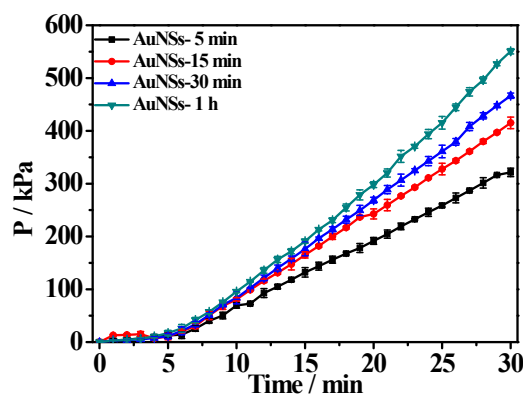


Figure S13. Pressure-change profiles of the H_2O_2 decomposition reaction with different surface areas of Au nanosheets catalase in 6.7% H_2O_2 solution ($[\text{catalase}]=0.4 \text{ mg}$). Values are expressed as mean \pm SD. As shown in Figure S13, the oxygen evolution rate of AuNSs-1 h is $27 \mu\text{mol}\cdot\text{mg}^{-1}\cdot\text{min}^{-1}$, which is higher than that of the AuNSs-30 min ($23 \mu\text{mol}\cdot\text{mg}^{-1}\cdot\text{min}^{-1}$), AuNSs-15 min ($21 \mu\text{mol}\cdot\text{mg}^{-1}\cdot\text{min}^{-1}$) and AuNSs-5 min ($16 \mu\text{mol}\cdot\text{mg}^{-1}\cdot\text{min}^{-1}$). Thus, the order of catalytic activities of Au nanostructures is AuNSs-1 h > AuNSs-30 min > AuNSs-15 min > AuNSs-5 min.

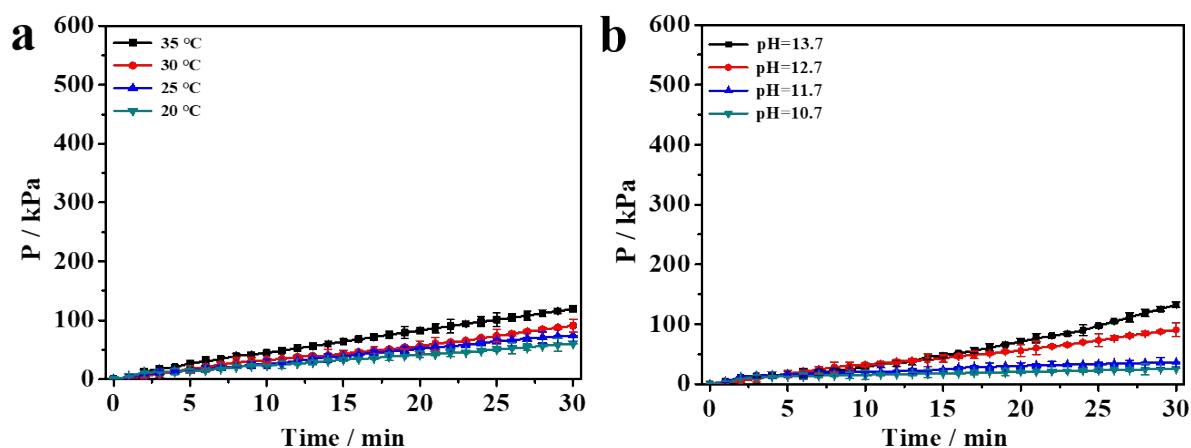


Figure S14. (a) Pressure-change profiles of the H_2O_2 decomposition reaction at different temperatures without catalase in 6.7% H_2O_2 solution. (b) Pressure-change profiles of the H_2O_2 decomposition reaction at different pH value without catalase in 6.7% H_2O_2 solution. Values are expressed as mean \pm SD. As shown in Figure S14, the decomposition of alone H_2O_2 is very little influenced by the temperature and pH. Only when the Au nanosheets exist, the decomposition of H_2O_2 is affected by the temperature and pH.

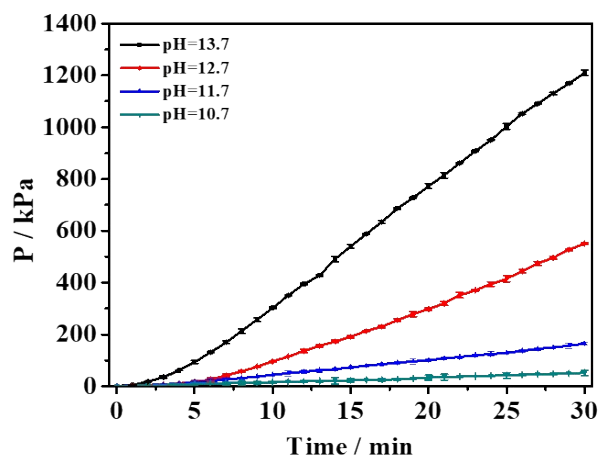


Figure S15. Pressure-change profiles of the H₂O₂ decomposition reaction at different pH value with AuNSs-5 catalase in 6.7% H₂O₂ solution ([catalase]=0.4 mg). Values are expressed as mean \pm SD.

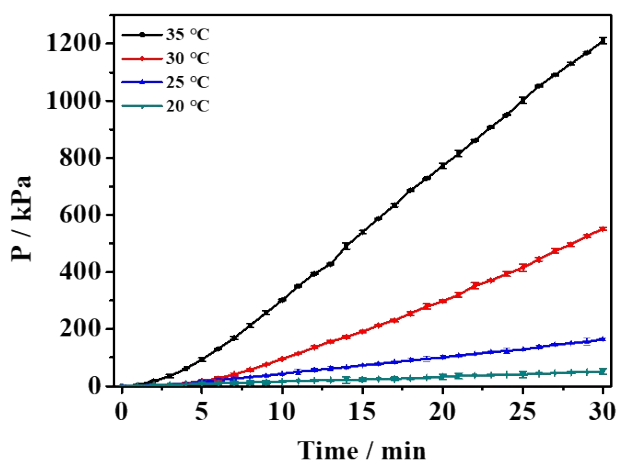


Figure S16. Pressure-change profiles of the H₂O₂ decomposition reaction at different temperatures with AuNSs-5 catalase in 6.7% H₂O₂ solution ([catalase]=0.4 mg). Values are expressed as mean \pm SD.

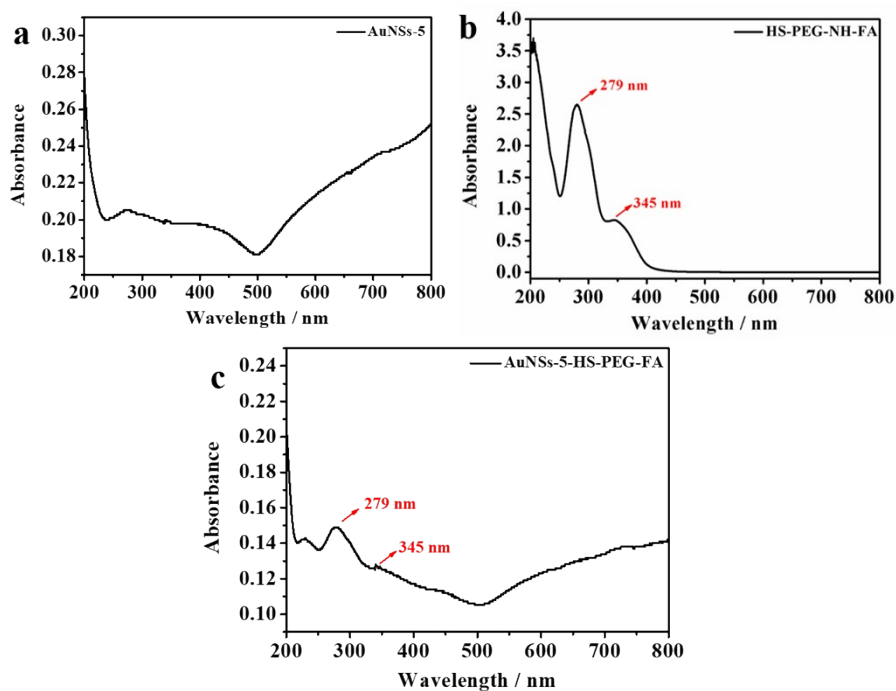


Figure S17. UV-vis absorption spectrum of (a) AuNSs-5; (b) HS-PEG-NH-FA; (c) AuNSs-5-HS-PEG-NH-FA. As shown in Figure S17b, the absorption peaks at 273 nm and 350 nm belong to folic acid (FA).⁵ And the absorption peaks of FA also exist in AuNSs-5-HS-PEG-NH-FA. This indicates that the FA was attached to the AuNSs-5.

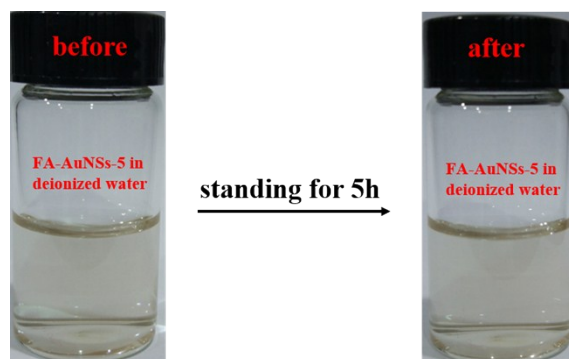


Figure S18. Photographs of FA-AuNSs-5 dispersed in deionized water. As shown in Figure S18, FA-AuNSs-5 is well dispersed in water and there is no aggregation after standing for 5h. This indicates the FA-AuNSs-5 have excellent dispersibility in deionized water.

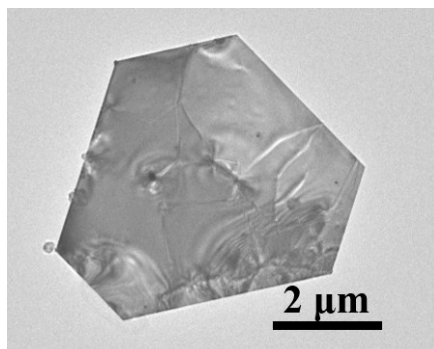


Figure S19. TEM images of FA-AuNSs-5 dispersed in deionized water. As shown in Figure S19, the FA-AuNSs-5 in deionized water are monodisperse and without aggregation.

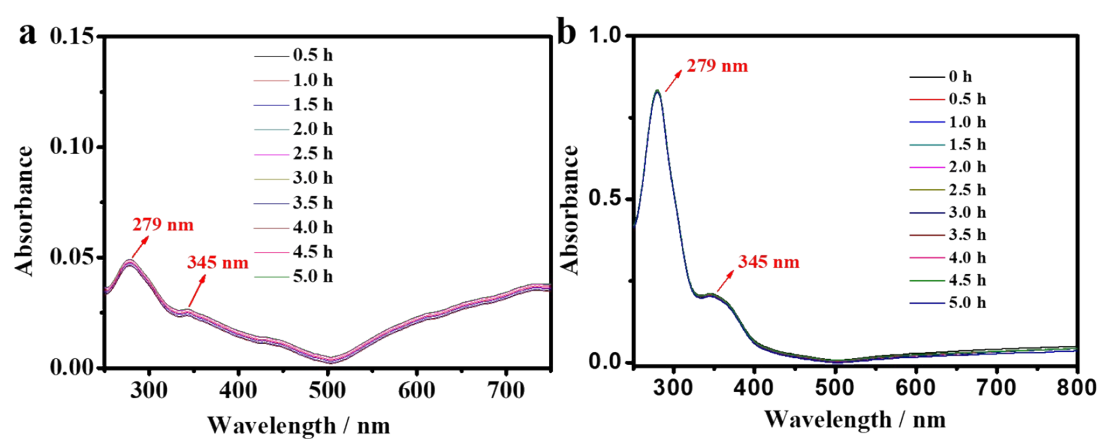


Figure S20. UV-vis detection of FA-AuNSs-5 in deionized water (a) and in the serum (b) at different times. As shown in Figure S20a, the absorption peaks at 279 nm and 345 nm belong to folic acid (FA) and the absorption intensity of peaks scarcely changes within 5h. And the higher intensity of the absorption peaks at 279 nm in the Figure S20b is because the serum also has the absorption peak at 279 nm. This indicates that FA-AuNSs-5 has good dispersion in water and has no aggregation.

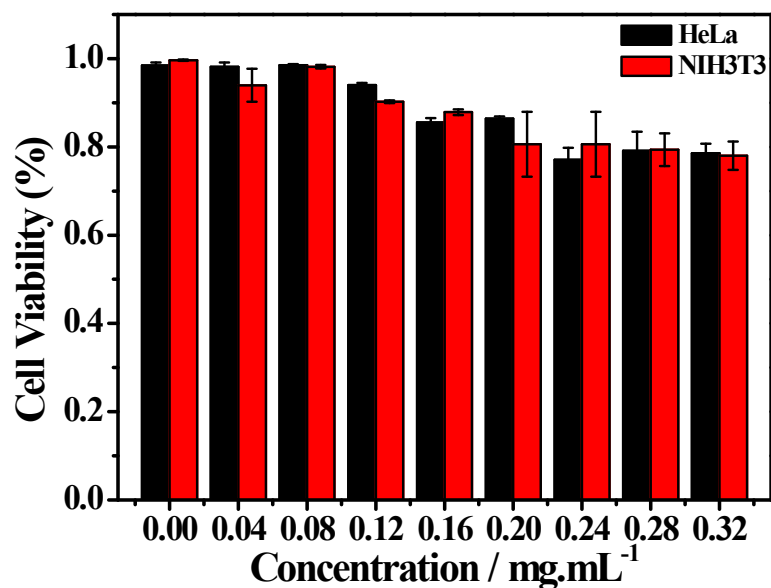


Figure S21. Cell viability of HeLa and NIH3T3 cells incubated with FA-AuNSs-5 with different concentrations (0, 0.04, 0.08, 0.12, 0.16, 0.20, 0.24, 0.28, 0.32 $\text{mg}\cdot\text{mL}^{-1}$) for 48 h at 37 °C. Values are expressed as mean \pm SD. As shown in Figure S20, the cell viabilities of the HeLa and NIH3T3 cells were still greater than 75% after 48 h, which indicates that FA-AuNSs-5 exhibits low toxicity on the cells.

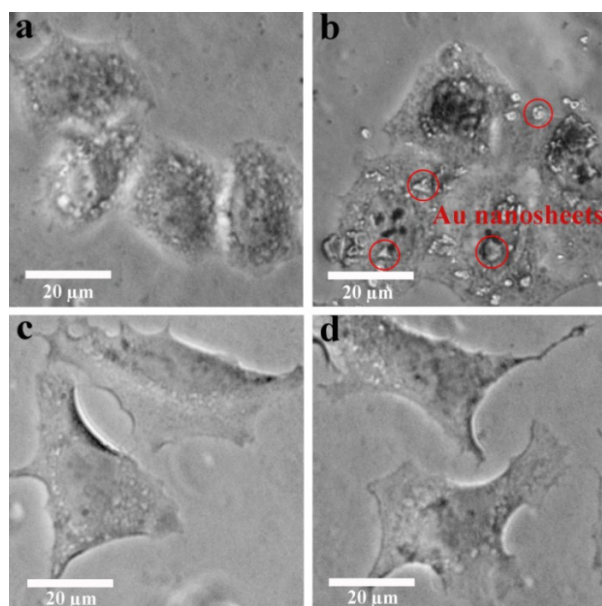


Figure S22. Confocal images of (a) HeLa cells alone; (b) HeLa cells incubated with FA-AuNSs-5; (c) NIH3T3 cells alone; and (d) NIH3T3 cells incubated with FA-AuNSs-5.

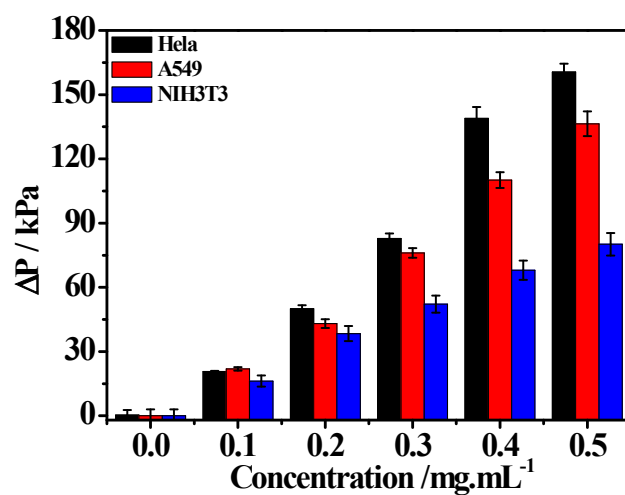


Figure S23. Pressure change profiles of cells incubated with FA-AuNSs-5 for 1 h. Values are expressed as mean \pm SD.

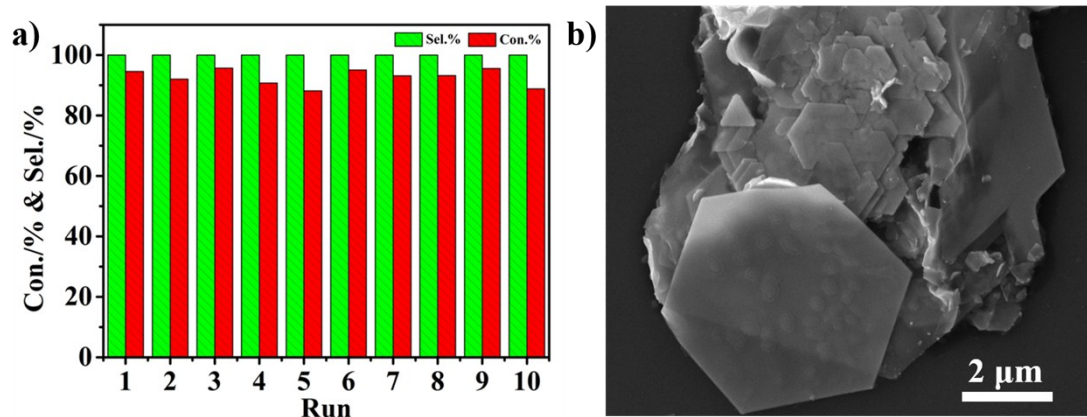
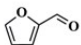
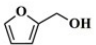
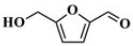

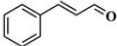
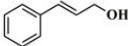
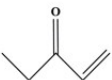
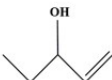


Figure S24. (a) Recycling results for selective catalytic hydrogenation reactions of furfural using AuNSs-5 catalyst. Reaction conditions: 10 μ L of furfural, 2 mg of AuNSs-5 catalyst in 10 mL of isopropyl alcohol containing 10 mg of KOH, 60 $^{\circ}$ C for 4 h. (b) The SEM images of AuNSs-5 after ten runs.

Table S1. Selective catalytic hydrogenation of α,β -unsaturated aldehydes over Au nanosheets catalyst

Entry	Reactant	Main product	Conv.(%)	Select.(%)
1			98	100
2			73	100
3			88	100
4			79	100

Reaction conditions: 10 μ L of reactant, 2 mg AuNSs-5catalyst in 10 mL of isopropyl alcohol containing of 10 mg of KOH. The reaction temperature was set at 60 $^{\circ}$ C and controlled by an oil bath. The mixture was stirred for 4h at 700 rpm using magnetic stirrer during the reaction.

References.

- 1 Z. H. Tang, B. Xu, B. H. Wu, M. W. Germann and G. L. Wang, *J. Am. Chem. Soc.*, 2010, **132**, 3367-3374.
- 2 J. Liu, X. Huo, T. R. Li, Z. Y. Yang, P. X. Xi, Z. Y. Wang and B. D. Wang, *Chem. Eur. J.* 2014, **20**, 11549-11555.
- 3 M. J. Hostetler, J. J. Stokes and R. W. Murray, *Langmuir* 1996, **12**, 3604-3612.
- 4 Z. Y. Wang, J. Liu, T. R. Li, J. Liu and B. D. Wang, *J. Mater. Chem. B.*, 2014, **2**, 4748-4753.